HHS Public Access

Author manuscript

Clin Cancer Res. Author manuscript; available in PMC 2024 October 01.

Published in final edited form as:

Clin Cancer Res. 2024 April 01; 30(7): 1293–1306. doi:10.1158/1078-0432.CCR-23-3647.

Development of a [^{89}Zr]Zr-labeled human antibody using a novel phage-displayed human scFv library

Abhay K. Singh[1], **Calvin D. Lewis**[1], **Cristian AWV Boas**[1], **Philipp Diebolder**[1], **Prashant N. Jethva**[2], **Aaron Rhee**[1], **Jong Hee Song**[3], **Young Ah Goo**[3], **Shunqian Li**[4], **Michael L. Nickels**[5,6], **Yongjian Liu**[5], **Buck E. Rogers**[1,7], **Vaishali Kapoor**[1,7,*], **Dennis E. Hallahan**[1,7,*]

[1]Department of Radiation Oncology, Washington University School of Medicine, St. Louis, MO, USA.

[2]Department of Chemistry, Washington University in St. Louis, Saint Louis, MO, USA

[3]Mass Spectrometry Technology Access Center at the McDonnell Genome Institute (MTAC@MGI), Washington University in St. Louis, Saint Louis, MO, USA

[4]Department of Medicine, Washington University in St. Louis, Saint Louis, MO, USA

[5]Mallinckrodt Institute of Radiology, Washington University in St. Louis, Saint Louis, MO, USA

[6]Cyclotron Facility, Mallinckrodt Institute of Radiology, Washington University School of Medicine, St. Louis, MO, USA

[7]Siteman Cancer Center, St. Louis, MO, USA

Abstract

Purpose: Tax-interacting protein 1 (TIP1) is a cancer-specific radiation-inducible cell surface antigen that plays a role in cancer progression and resistance to therapy. This study aimed to develop a novel anti-TIP1 human antibody for noninvasive PET imaging in cancer patients.

Experimental Design: A phage-displayed scFv library was created from healthy donors' blood. High-affinity anti-TIP1 scFvs were selected from the library and engineered to human IgG1. Purified antibodies (Abs) were characterized by size-exclusion chromatography-HPLC (SEC-HPLC), native mass spectrometry (native MS), ELISA, BIAcore, and flow cytometry. The labeling of positron emitter [^{89}Zr]Zr to the lead Ab, L111, was optimized using deferoxamine

[*]**Co-Corresponding authors:** Vaishali Kapoor, Cancer Biology Division, Department of Radiation Oncology, Washington University in St. Louis, 4511 Forest Park, St. Louis, MO, 63108, Phone (314) 362-9914; Fax. (314) 362-9790 vkapoor@wustl.edu; Dennis E Hallahan, Department of Radiation Oncology, Washington University in St. Louis, 4511 Forest Park, St. Louis, MO, 63108, Phone: 314-362-9700, Fax: 314-747-5498, dhallahan@wustl.edu.

Author contributions:

AKS and VK developed the hypothesis, designed the studies, performed research, analyzed the data, and wrote the manuscript. CDL, CAWVB, PD, AR, and JHS performed experiments and analyzed data. PNJ, YAH, and JHS performed native MS experiments. MLN and YL provided helpful advice, discussed data, and reviewed the manuscript. CAWVB and BER designed the radioactivity studies and analyzed the data. DEH reviewed the manuscript, developed the hypothesis, provided funding, and supervised the project. All authors reviewed the manuscript and contributed to discussions.

Conflicts of interest: Dr. Dennis Hallahan is the founder of MedGyde LLC. Dr. Abhay K Singh and Dr. Vaishali Kapoor are consultants for MedGyde LLC. Dennis Hallahan, Vaishali Kapoor, and Abhay K Singh are inventors on pending patents (WO2023287941A2). Dr. Shunqiang Li has received a license fee from Inotiv, Inc.

(DFO) chelator. The stability of [^{89}Zr]Zr-DFO-L111 was assessed in human serum. Small animal PET studies were performed in lung cancer tumor models (A549 and H460).

Results: We obtained 95% pure L111 by SEC-HPLC. Native MS confirmed the intact mass and glycosylation pattern of L111. Conjugation of 3 molar equivalents of DFO led to the optimal DFO-to-L111 ratio of 1.05. Radiochemical purity of 99.9% and specific activity of 0.37 MBq/μg was obtained for [^{89}Zr]Zr-DFO-L111. [^{89}Zr]Zr-DFO-L111 was stable in human serum over seven days. The immunoreactive fraction in cell surface binding studies was 96%. In PET, preinjection with 4 mg/kg cold L111 before [^{89}Zr]Zr-DFO-L111 (7.4 MBq; 20 μg) significantly ($P<0.01$) enhanced the tumor-to-muscle SUVmax ratios on day 5 compared to day 2 post-injection.

Conclusions: L111 Ab targets lung cancer cells *in vitro* and *in vivo*. [^{89}Zr]Zr-DFO-L111 is a human antibody that will be evaluated in the first-in-human study of safety and PET imaging.

Keywords

TIP1; Radiopharmaceutical; Radiation; PET imaging; lung cancer; [^{89}Zr]Zr

Introduction

Ionizing radiation induces the endoplasmic reticulum (ER) stress response, resulting in membrane-dependent translocation of proteins to the cancer cell surface (1-4). We developed therapeutic antibodies that bind specifically to the inducible antigens on the cancer cell surface (5). Targeting radiation-inducible antigens is a new paradigm in cancer drug development that exploits cancer's exaggerated response to ionizing radiation.

TIP1 is a radiation-inducible cell surface protein specific to cancer (4,6-8). This inducible protein is a chaperone that binds to multiple protein binding partners through its PDZ domain (9). We found that the antibody to radiation-inducible TIP1 activates endocytosis, facilitating antibody-drug conjugate retention and drug dissociation within cancer cells (4,6). Cytotoxic agents that include chemotherapy or radiopharmaceuticals are conjugated to anti-TIP1 antibodies, which bind specifically to this inducible cancer antigen (6,10).

Positron emission tomography (PET) is a molecular imaging tool that can non-invasively detect cancer and monitor response to treatment. Antibody-based PET (ImmunoPET) has shown promising results in clinical trials for treatment guidance, recurrence monitoring, and visualizing the biodistribution of immune checkpoint inhibitors in lung cancer patients (11,12). With the goal of imaging patients undergoing external beam radiation therapy, we developed a human antibody that targets radiation-inducible TIP1.

We created a diverse phage-displayed human single-chain variable fragment (scFv) antibody library (WashU II) from non-immune healthy donors' blood. Biopanning of the WashU II phage-displayed library against the recombinant TIP1 protein isolated several target-specific scFvs, from which eight high-affinity antibodies (Abs) were selected to create human IgG1 antibodies. Antibody engineering technologies provided the reformatting of scFvs to full-length IgGs (13,14). We reformatted the eight scFvs to full-length human IgG1 antibodies and expressed them in suspension ExpiCHO-S™ Cells.

The present report describes the characterization of the lead antibody, which is intended for a clinical trial. We optimized the buffer, DFO to antibody ratio, and stability of antibody conjugates. Preclinical imaging studies showed binding within mouse models of lung cancer and liver clearance of the antibody conjugate. We determined that a DFO-to-antibody ratio of 1:1 achieved lower liver clearance and increased tumor binding as compared to a DFO-to-antibody ratio of three. We utilize positron emitter, [^{89}Zr]Zr, as the radiotracer because of its 78.4-hour half-life, which is well suited to monitor the long circulation time of IgG. Antibodies were radiolabeled using the chelator deferoxamine (DFO).

The findings of this study will serve as the basis for the chemistry and manufacturing component of the Investigational New Drug application with the FDA. We plan first in human clinical trials to study the safety of the anti-TIP1 antibody and determine which cancers are best suited to progress to therapeutic clinical trials. In the clinical trial, we propose to image the anti-TIP1 antibody-conjugated to the positron emitter, [^{89}Zr]Zr, and determine the pharmacokinetics and optimal schedule of delivery of radiation and antibody conjugate in patients receiving radiation therapy.

Materials and Methods

Cell lines, chemicals, and irradiation

Human NSCLC cell lines A549 (ATCC Cat# CCL-185, RRID:CVCL_0023), H460 (ATCC Cat# HTB-177, RRID:CVCL_0459), liver cancer cell lines Hep3B (ATCC Cat# HB-8064, RRID:CVCL_0326), HepG2 (ATCC Cat# HB-8065, RRID:CVCL_0027), head and neck cancer cell lines Cal27 (ATCC Cat# CRL-2095, RRID:CVCL_1107), and FaDu (ATCC Cat# HTB-43, RRID:CVCL_1218) were obtained from ATCC. A549 cells were cultured in DMEM/F-12; H460 in RPMI media; Hep3B and HepG2 in EMEM; Cal27 and FaDu in DMEM containing 10% fetal bovine serum (FBS) and 1% penicillin-streptomycin (P/S). All cell cultures were grown in a humidified incubator at 37°C with 5% CO_2. All the cell lines were tested for mycoplasma contamination using the MycoAlert™ PLUS Mycoplasma Detection Kit (Lonza) every three months and tested negative. All cell lines were disregarded after 15 passages from thawing. For *in vivo* injections, cells were used within ten passages from thawing. Short tandem repeat (STR) profiling was performed for all cell lines before beginning experiments. Ionizing radiation was delivered using an x-ray irradiator (RS 2000, Rad Source, USA) with an operating voltage and current of 160 kV and 25 mA, respectively. A dose rate of 0.0682 Gy/s and 0.0167 Gy/s was used for *in vitro* and animal radiation experiments, respectively. Mice were anesthetized with 2% isoflurane and placed in the irradiator with shielding of the body using lead. The target tissues (hindlimb tumors) were exposed during radiation for animal experiments.

WashU-II library preparation and biopanning

WashU-II phage display library was generated using blood samples from 54 healthy donors. Donor samples were acquired in accordance with the Declaration of Helsinki and approved by the Institutional Review Board of Washington University School of Medicine in St. Louis (HRPO#201611011). Written informed consent was obtained from all subjects involved in the study. RNA was isolated from peripheral blood mononuclear cells (PBMC) using the

RNeasy Kits (Qiagen Cat# 74104), and the cDNA was prepared using the High-Capacity cDNA Reverse Transcription Kit (Applied Biosystems Cat# 4368814). We used a set of 91 primers covering 117 human germline genes, according to the VBASE database. Human antibody repertoires (IgG and IgM) were amplified by PCR from the cDNA of mixed human PBMC samples and cloned randomly into a phagemid vector. This vector encodes for a 16 amino acid linker $(G4S)_3T$ between the VH and VL domain of the scFv and adds a C-terminal 6xHis and FLAG tag. A two-step cloning strategy (first LCs, then HCs) was used, similar to the one previously described (15). The VH repertories were first cloned by electroporation in E. coli TG1 (Lucigen, Cat# 60502), followed by cloning of the VL-kappa or VL-lambda repertories. The glycerol stocks were stored at −80 °C. Immunotubes were coated with full-length recombinant human TIP1 protein (Prospec, Cat# PRO-981), and biopanning was performed according to a protocol described previously (16). In brief, phages expressing the scFvs of the WashU-II library were prepared, and TIP1-specific scFvs were enriched during three rounds of selection using an acid solution for elution.

Monoclonal ELISA of soluble scFv antibody fragments

After three rounds of biopanning, TIP1-specific phage-displayed scFvs were selected by monoclonal ELISA. In brief, *E. coli* strain HB2151 (gift from Dr. Buck Roger's lab, Washington University in St. Louis) was cultured, infected with round three phages, and plated on 2xYT agar plates containing 100 μg/mL ampicillin and 1% glucose. The next day, single colonies were inoculated into 2xYT media containing 100 μg/mL ampicillin and 1% glucose in 96-well plates and grown overnight. An expression plate was prepared in a separate 96-well plate by inoculating overnight grown E. coli HB2151 in 2xYT media containing 100 μg/mL ampicillin and 1% glucose. After OD^{600nm} reached 1.0, bacteria were centrifuged, resuspended in 2xYT supplemented with 100 μg/mL ampicillin and 0.5 mmol/L IPTG, and incubated for 16 hours at 30°C to allow scFv production. Nunc MaxiSorp 96-well plates were coated with 10 μg/mL of TIP1 protein in phosphate-buffered saline (PBS) overnight. After blocking with 2% non-fat milk in PBS (MPBS) for 2 hours, the bacterial supernatants containing soluble scFvs were added to wells and incubated for 1 hour at room temperature. Unbound scFvs were washed away. Horseradish peroxidase-conjugated anti-His tag IgG (Jackson ImmunoResearch Labs Cat# 300-035-240, RRID: AB_2892160) was used as a secondary antibody. ELISA was developed using the TMB substrate kit (ThermoFisher, Cat# 34021).

scFv engineering to full-length IgG

Selected lead scFvs were sequenced and cloned to generate full-length IgGs. In this protocol, we make use of the pTRIOZ expression vector (InvivoGen, Cat# ptrioz-higg1). It consists of three cassettes encoding the expression of the mAb heavy chain, light chain, and antibiotic selection with Zeocin. Each cassette is under the control of a unique composite promotor for optimal expression. VH and VL sequences were cloned upstream of the heavy and light chain constant regions, respectively. The signal sequence was added at a 5' sequence of both heavy and light chain variable regions.

Expression and purification of IgG

Endotoxin-free plasmid DNA was prepared using the PureLink™ Expi Endotoxin-Free Maxi Plasmid Purification Kit (Invitrogen, Cat# A31231) for large-scale expression of the IgG. We used ExpiCHO-S™ Cells (ThermoFisher Scientific, Cat# A29133) for high transient expression levels. We used the single plasmid to transfect for maximization of recombinant antibody yields. In the cassette, the composite promotor (AldA enh/hFerH) combines the human aldehyde dehydrogenase enhancer and core promotor of the human ferritin heavy chain gene. In cassette 2, the composite promotor (hCMV enh/hFerL) combines the human cytomegalovirus (CMV) immediate-early gene one enhancer and the core promotor of the human ferritin light chain gene. Cell supernatants were harvested to purify recombinant antibodies via HiTrap MabSelect PrismA column (Cytiva, Cat# 17549853) on an ÄKTA pure™ 25 M system (Cytiva, Cat# 29018226) with Unicorn 7.0 software (Cytiva, Cat# 29128116-PMO) using PBS as a running buffer at a constant flow rate of 1.0 ml/min. The Protein A purified antibodies were further purified using gel filtration chromatography. The antibody was loaded on a Superdex 200 10/300 GL column (Cytiva, Cat# 17-5175-01). Gel Filtration standards (BioRad, Cat# 1511901) were used as molecular weight controls. The purity and molecular mass of the purified antibody were analyzed on Coomassie gel using standard procedures.

Antibody integrity by CE-SDS

Non-reduced and reduced Capillary electrophoresis sodium dodecyl sulfate (CE-SDS) analyzed purified antibody integrity on a Perkin Elmer LabChip GXII Touch HT. The Protein Express High Sensitivity Antibody Analysis 200 method was used per the manufacturer's protocol. Anti-TIP1 antibody was analyzed at 0.5 mg/mL concentration in a 96-well plate. The non-reduced samples were diluted in PBS-10 mM N-Ethylmaleimide (NEM); 5 µL of the sample at 0.5 mg/mL was added to a 7 µL Protein Express Sample Buffer. The sample was incubated at 70°C for 10 minutes. 32 µL of water was added to each sample, and the samples were centrifuged at 1200 x g for 2 minutes before analysis. The reduced sample was prepared in the same manner with 7 µL sample denaturing solution added instead of sample buffer solution and 0.5 mg/mL samples diluted in PBS. The sample denaturing solution consisted of 24.5 µL of 1M Dithiothreitol (DTT) added to 700 µL Protein Express Sample Buffer. Analysis was performed using LabChip GX Reviewer software for quantification.

SEC-HPLC

Chromatographic separation was performed using an Agilent AdvanceBio size exclusion chromatography (SEC) column (300Å 2.7 µm 4.6 x 300 mm) connected to a Dionex Ultimate 3000RS HPLC system (ThermoFisher Scientific, Hemel Hempstead, UK). The method consisted of an isocratic elution over 15 minutes with a mobile phase comprising 150 mM sodium phosphate pH 6.9. The flow rate was 0.35 mL/minute, and detection was carried out by UV absorption at 280 nm.

Cation exchange chromatography

Cation exchange chromatography was performed using a YMC BioPro IEX SF (5 μm, L x ID = 100 x 4.6 mm) column connected to a Dionex Ultimate 3000RS HPLC system (ThermoFisher Scientific, Hemel Hempstead, UK). Mobile phases comprised (A) 20 mM 2-(N-morpholino) ethanesulfonic acid (MES), pH 5.7, and (B) 20 mM MES, 2 M sodium chloride (NaCl), pH 5.7. Chromatography was accomplished using the following gradient: 1.5% B to 30% B over 23 minutes at a 0.3 mL/min flow rate. Elution was monitored by UV absorption at 280 nm. Samples were diluted to 1 mg/mL with mobile phase A, and 10 μg injections were made.

Antibody glycan profiling

Hydrophilic interaction liquid chromatography (HILIC) combined with fluorescence detection (FLD) analysis of Fc N-Glycan profiles and major glycans distribution. Briefly, 15 μg of the purified antibody was deglycosylated using PNGase F (Waters, Elstree, UK), and the released glycans were labeled with RapiFluor-MS reagent (Water, Elstree, UK) before being analyzed by HILIC-FLD using a Dionex U3000 UHPLC (Thermo Fisher Scientific, Loughborough, UK) equipped with an ACQUITY UPLC glycoprotein BEH amide column (Waters, Elstree, UK). A dextran reference standard (Waters, Elstree, UK) was included before and after each batch. The chromatograms were analyzed using Chromeleon™ Software (ThermoFisher Scientific, Loughborough, UK), and the assignment of individual glycoform peaks was achieved by alignment with the glycan profile of an injection of three standards (PTS, High Mannose, Sialylated).

ELISA

The functional affinity of the anti-TIP1 antibodies to recombinant TIP1 protein was measured using ELISA. Recombinant human TIP1 protein at 10 μg/mL in PBS (100 μL/well) was coated on ELISA plates and incubated overnight at 4°C. Plates were blocked with a blocking reagent (5% milk in PBS-0.1% tween 20) for 2 hours. The L111 antibody, DFO-L111, and [^{89}Zr]Zr-DFO-L111 (5 nM) were four-fold serially diluted and added to ELISA plates for 1 hour at room temperature. The plate was washed three times with PBS-0.1% tween20. Anti-human IgG–HRP conjugated secondary antibody (Sigma, Cat# AP309P, RRID: AB_11212373) diluted in 5% milk in PBS-0.1% tween at 100 μL/well was added for 1 hour at room temperature. The ELISA plate was washed three times with PBS-T and three times with PBS. After the washes, 100 μL of TMB substrate (ThermoFisher, Cat# 34021) was added to each well. The reaction was quenched by adding 100 μL/well sulfuric acid (2N). The absorbance was read at 450 nm using a spectrophotometer.

Surface Plasmon Resonance for affinity analysis

The functional affinity of the anti-TIP1 IgGs for TIP1 protein was measured by the biosensor-based surface plasmon resonance (SPR) technique using an automatic apparatus BIAcore T200 (Cytiva, Cat# 28975001, RRID: SCR_019718) as we described earlier (17-19). Recombinant human or mouse TIP1 protein (ligand) was immobilized on the surface of the CM5 sensor chip (Cytiva, Cat# 29104988) using the amine coupling wizard. The reference surface was activated with EDC/NHS and blocked with ethanolamine. The

concentrations of anti-TIP1 IgGs passed over human TIP1 were 0.13, 0.41, 1.23, 3.7, 11.1, and 33.3 nM. Reference subtracted sensograms were fitted using the BIA evaluation software (Cytiva, Cat# 28981619, RRID: SCR_015936), and K_D was calculated.

Antigen-Antibody docking

Protein (TIP1-PDB: 3DIW) and antibody structure (model) were processed using Schrödinger's Biologics Suite (RRID: SCR_014879). The protein preparation wizard automatically adds missing hydrogen atoms and correct metal ionization states to ensure proper formal charge and force field treatment and removes co-crystallized water molecules. The software has a restrained minimization that allows hydrogen atoms to be freely minimized while allowing for sufficient heavy-atom movement to relax strained bonds, angles, and clashes. The protein-protein docking application was opened in Schrödinger Biologic, the software's antibody and antigen energy minimized structure was uploaded, and the wizard ran. The 1.2 Å grid cell size defines the sampling. The energy-like scoring function describes the receptor-ligand interactions and is efficiently calculated using Fast Fourier transforms. Results were clustered with a 10 Å cube size, and one or several lowest energy translations for the given rotation were retained. Finally, results from different rotations were collected and sorted. The result was analyzed using a protein interaction panel in the Biologics Suite in Schrödinger.

Flow cytometry

Cell surface binding of the human anti-TIP1 IgG antibodies was analyzed on cancer cells. An Anti-human PE secondary antibody was obtained from Biolegend (Biolegend, Cat# 410708, RRID: AB_2565786). For analysis, cells were incubated with antibodies in FACS staining buffer (PBS containing 5% (vol/vol) FBS and 0.1% sodium azide). Flow cytometry was performed on a MACSQuant Analyzer flow cytometer (RRID: SCR_020268). The expression level was presented as median fluorescence intensity minus the secondary antibody control.

In-silico immunogenicity (Epibase-Lonza)

We used Epibase™ software to calculate a quantitative estimate of the free energy of binding ΔG_{bind} of a peptide for each of the available HLA class II receptors. Free energies were converted into Kd-values through $\Delta Gbind = RT \ln(Kd)$. Peptides were classified as strong (S), medium (M), or non-binders (N). The threshold values used were specific for each allotype. Peptides, an exact match for self-peptides, were analyzed separately. Critical epitopes were defined as any strong DRB1, DRB3/4/5, DQ, and DP binder and any medium-strength DRB1 and DRB3/4/5 binder. The binder represents the subset of epitopes considered relevant in contributing to the immunogenic potential. The frequencies of the 85 major histocompatibility complex (MHC) class II allotypes in the global population were calculated using literature and public databases. The values indicate the percentage of individuals expressing a particular allotype. For each 10-mer peptide, a search was conducted for an identical match on TCR-facing residues. A match to the 10-mer peptide was found for all affected allotypes; it was completely filtered out. Peptides, either fully or partially filtered by the T-cell receptor (TCR)-facing filter, were referred to as TCR-filtered peptides. The TCR-facing filter was applied only to peptides that had not previously been

filtered as self-peptides. DRB1 SCORES: The DRB1 risk score of a protein/peptide is an approximate score representing a worst-case immunogenic risk and was calculated as a sum of the number of critical epitopes affecting a particular HLA allotype multiplied by the population frequency of the affected allotype. The sum was taken over all DRB1 allotypes used in the study.

NIR imaging

All animal studies were performed following the guidelines of the IACUC and with protocols approved by the Washington University Division of Comparative Medicine. The anti-TIP1 antibody or isotype control antibody (human IgG1, BioXcell, Cat# BE0297) was labeled with IRDye 800CW per the manufacturer's instructions (LI-COR, Cat# 929-70020). A patient-derived xenograft (PDX from a male patient with adenocarcinoma in the lungs) was implanted in the right flanks of NOD.Cg-*Prkdc*^{scid} *Il2rg*^{tm1Wjl}/SzJ mice (The Jackson Lab, Strain # 005557, RRID: IMSR_JAX:005557). The tumors were irradiated with 3 Gy or 0 Gy (sham-irradiated). The tumor-bearing mice were injected with 10 μg labeled antibodies via the tail vein. In some experiments, 0, 0.4, 4, and 40 mg/kg of unlabeled L111 antibody were injected prior to IRDye 800 labeled L111. The mice were anesthetized with 2% isoflurane for optical imaging and imaged using the Pearl Trilogy small animal imaging system (LI-COR). Fluorescence was detected using an 800nm channel with an excitation of 785 nm and an emission of 820nm. Animals were imaged at 0, 2, 4, 24, and 48 h following antibody injection. Images were analyzed using the Image Studio software (RRID: SCR_015795). Background subtracted signal intensity was plotted using Graph Pad Prism software (RRID: SCR_002798). For the NIR imaging-based biodistribution study, organs were harvested from tumor-bearing nude mice at five days post-injection, and data are represented as Signal intensity per organ weight in gm.

DFO conjugation to IgG

The anti-TIP1 antibody was conjugated to p-SCN-Bn-Deferoxamine (DFO) chelator (Macrocyclics, Cat# B-705) using a protocol previously described (20) with slight modifications. The anti-TIP1 antibody was buffer exchanged (Chelex-treated 0.1 M sodium carbonate/bicarbonate, pH 9.0) using a 5 ml Zeba spin column 40 kDa cutoff (Thermo Fischer scientific, Cat# 87767). Subsequently, 2.2 mg aliquots of antibody were combined with one, two, three, four, and ten molar equivalents of DFO in DMSO stock solution (10 mg/mL). These immunoconjugates were named D1, D2, D3, D4, and D10 (D = DFO, numeric value = molar equivalents of DFO conjugated), but these numbers do not indicate the actual number of conjugated chelators. The antibody and DFO mixture were allowed to react for 1 h at 37 °C in a thermomixer agitated at 600 rpm. The reaction mix was purified by 5 ml Zeba spin column 40 kDa cutoff and exchanged to Chelex-treated 1.0 M 4-(2-hydroxiethyl)-1-piperazineethanesulfonic acid (HEPES) pH 7.2 buffer. Pierce™ Bicinchonic acid (BCA) assay (ThermoFisher Scientific, Cat# 23227) for protein quantification was performed, and 200 μg aliquots of each Ab-DFO conjugate were snap-frozen and stored at −80 °C until radiolabeling. Mass spectrometry was performed to evaluate the number of DFO attached to the antibodies.

Native-MS analysis to elucidate the DFO-to-antibody ratio

Purified human IgG1 antibody-DFO conjugate was buffer exchanged with 200 mM ammonium acetate (99.99%, Millipore Sigma, Saint Louis, MO) buffer solution (pH 7) six times using Amicon Ultra-0.5 centrifugal Filter RC 30 kDa molecular weight cut off (Millipore Sigma Saint Louis, MO) at 10000 rcf and final sample solution was adjusted after measuring the protein concentration with NanoDrop. Approximately 4 μL of the sample was loaded into a platinum-coated emitter (Thermo Scientific, Waltham, MA) and electrosprayed directly into the mass spectrometer via a nanoESI source. Two mass spectrometers were used, and their data collection settings are described. Exploris 480 Orbitrap mass spectrometer (Thermo Scientific, RRID: SCR_022215) with Biopharma extended mass range option was used to obtain the native mass spectrum of the DFO-conjugated antibody with the following settings: capillary voltage of 1.5 kV, the capillary temperature of 80 °C, in-source CID of 70 V, and HCD collision energy of 100 V. The AGC target was set to 5 e^6. The mass resolving power was 120,000 at m/z = 400. Data processing was done using Thermo Xcaliber Qual Browser 4.0. Thermo Exactive Plus EMR Orbitrap mass spectrometer (Thermo Scientific, Waltham, MA) was used to obtain the native MS of the DFO-conjugated antibody with the following settings: capillary voltage of ~1.5 kV, in-source CID of 70 V, and HCD collision energy of 100 V, AGC target was set to 1 e6, mass resolving power was 17500 at m/z = 200 and other MS parameters were set for optimum transmission of ~150 kDa species. Data were processed using Thermo Xcaliber Qual Browser and Intact Mass (Protein Matrix Inc, Cupertino, CA).

Labeling with [^{89}Zr]Zr

For all radiolabeling reactions, aliquots of [^{89}Zr]Zr-oxalate were neutralized to ~pH 7.0–7.4 using Chelex-treated 1.0 M HEPES pH 7.2 and subsequently mixed with DFO–L111 Ab samples. The pH of the reaction mixtures was evaluated in the range of 6.9-7.2. The reaction mixture was incubated for 60 min at 37 °C at 300 rpm.

iTLC

Radiochemical yields were evaluated after 1 h of radiolabeling by radioiTLC [50 mM Diethylenetriamine pentaacetate (DTPA), pH 6.0 mobile phase] using silica-gel impregnated glass-microfiber paper strips (iTLC-SG, Varian, Lake Forest, CA) (analyzed by AR-2000, Bioscan Inc., Washington, DC).

Immunoreactivity assay

The immunoreactive fraction (%IRF) of [^{89}Zr]Zr-DFO-immunoconjugate was determined using a cell-based radioligand binding assay. The radiolabeled antibody was diluted in a 1% bovine serum albumin (BSA) solution such that 50 μl contains about 10,000 cpm using a gamma counter. A suspension containing 5x10^6/ml cells was prepared in PBS, and various volumes (500, 400, 300, 250, 200, 150, 50, 0 μl) were added to microcentrifuge tubes. 50 μl activity was added to all tubes except the background. PBS was used to make up the volume to 550 μl for all tubes. The samples were incubated at room temperature for 60 min in a mixer at 300 rpm. Subsequently, the cells were pelleted by centrifugation (600 g for 2 min), and the supernatant was discarded. Without resuspending, the cell pellets were washed

three times with ice-cold PBS (1 mL) with centrifugation (600 g, for 2 min) between each wash. Each tube was measured in an automated gamma counter (PerkinElmer). The activity data were background-corrected, and the amount of activity (antibody) bound to the cells was compared to the total amount of activity present. The % immunoreactive fraction (IRF) was determined by dividing the amount of radioactivity bound to the cell pellet by the total amount of radioactivity present in the cell pellet.

In vitro serum stability

In vitro serum stability of the [^{89}Zr]Zr-DFO-L111 antibody was performed to determine whether the compounds radiolabeled with [^{89}Zr]Zr^{4+} remained stable in the human serum. Ten microliters (7.4 MBq [~200 μCi]) of [^{89}Zr]Zr-DFO-L111 antibody was added to 90 μL of human serum and incubated at 37°C with agitation (300 rpm). Aliquots were removed at each time point (1, 2, 5, and 7 days) and analyzed using instant thin-layer chromatography with 50 mM DTPA pH 6.0 solution as the mobile phase. All reactions were conducted in triplicate, and data were plotted using GraphPad Prism software (RRID: SCR_002798).

Biodistribution with [^{89}Zr]Zr-DFO-L111

All animal experiments were conducted according to the guidelines of the Institutional Animal Care and Use Committee (IACUC) and approved by the Washington University Animal Studies Committee. Nude mice were injected with 100 μL of 3 ×10^7 cells/mL A549 cells. Tumors were allowed to grow for three weeks until they were palpable. Tumor sizes ranged from 300-500 mm^3. Mice bearing tumors were irradiated with three doses of 3 Gy and injected via tail-vein with [^{89}Zr]Zr-DFO-L111 or [^{89}Zr]Zr-isotype control Ab (human IgG1, BioXcell, Cat# BE0297) (0.37 MBq; 5 μg). For the tumor-blocking studies, 40 mg/kg of unconjugated L111 antibody was injected before the injection of [^{89}Zr]Zr-DFO-L111. Mice were sacrificed on days 2 and 5 post-injection, and organs were harvested, weighed, and assayed in the gamma counter for biodistribution studies. Radioactivity associated with each organ was expressed as a percentage of the injected dose per gram of organ (% ID/g).

Small animal PET Imaging and Post-PET Biodistribution

Mice bearing H460 or A549 tumors were irradiated with three doses of 3 Gy and injected via tail-vein with [^{89}Zr]Zr-DFO-L111 (7.4 MBq; 20 μg). The specific activity of [^{89}Zr]Zr-DFO-L111 was 0.37 MBq/μg. Static PET images were acquired for 20 min on day 2 and 30 min on day 5 post-injection using an Inveon PET/CT scanner (Siemens, Knoxville, TN). To block uptake in normal tissues, 4 mg/kg of unconjugated L111 was injected 10 min before injection of [^{89}Zr]Zr-DFO-L111. The mice were euthanized on day 5, and post-PET biodistribution was performed as described above. The PET images were reconstructed using the maximum a posteriori probability (MAP) algorithm and coregistered with CT images using image display software (Inveon Research Workplace Workstation, Siemens, Schenectady, NY). Regions of interest (ROI) were drawn for tumor uptake and analyzed as standard uptake values (SUV) using the formula SUV = (MBq/mL) × (animal weight (g))/injected dose (MBq).

Statistical analysis

Statistical analyses were performed using the Student's t-test and or one-way or two-way analysis of variance (ANOVA). All analyses were performed using GraphPad Software (RRID: SCR_002798), and statistical significance is indicated in each graph where appropriate.

Data availability statement

The data generated in this study are available upon request from the corresponding author.

Results

Human scFv Phage display library generation

A vastly diverse phage-displayed human antibody library (WashU-II library) was created for the isolation of high-affinity scFv antibodies to target proteins (Suppl. Figure 1). This library was generated by optimizing the individual steps of library construction to increase the efficiency of cloning the scFv nucleotide sequence. First, the pooled VH repertoire was cloned into the phagemid vector encoding for a 16 aa linker $(G_4S)_3T$ and C-terminal 6XHis and Flag tag, followed by cloning of the pooled kappa and lambda VL repertoires, respectively. The final size of the WashU-II library was 3 x 10^9 distinct scFv antibodies. This library includes 22 antibody families and 117 antibody germlines. The PCR of the library is shown in Supplemental Figure 2. Western blot analysis of the resulting WashU II phage-displayed scFv antibodies was probed with an anti-pIII antibody. We found that the cloned scFv repertoire was fused to the pIII coat protein of the M13 phage (Suppl. Figure 2B). Similarly, the western blot probed with an anti-Flag antibody confirmed a high percentage of complete scFv-pIII fusion proteins on the surface of the WashU-II phages used for biopanning towards TIP-1 protein (Suppl. Figure 2C).

anti-TIP1 human scFv discovery and engineering into full-length IgG

Figure 1A shows a schematic representation of the antibody discovery and engineering methods using the WashU II library. We performed three rounds of biopanning against the recombinant human TIP1. Polyclonal phage ELISA shows enrichment of TIP1-specific scFvs during the selection rounds and no binding against milk, lysozyme, and BSA (Figure 1B). A representative DNA gel confirmed the full-length of isolated scFvs at ~900 bp (Figure 1C). After three rounds of biopanning, the enriched polyclonal TIP1-specific phage pool was screened for monoclonal phage-displayed scFvs by ELISA. Monoclonal phage ELISA identified positive anti-TIP1 scFv binders (Figure 1 D-E). All positive binders were sequenced, and eight unique scFvs were selected for IgG1 cloning. All eight scFvs were converted to IgGs by cloning the respective V_H and V_L sequences into the pTRIOZ expression vector, followed by transient expression of IgGs in ExpiCHO-S™ Cells.

Selection of a lead human IgG1 against TIP1

The ExpiCHO-S™ Cell supernatants containing the full-length antibodies were purified by affinity chromatography using a protein A column (Suppl. Figure 3A). The antibodies were further purified using size-exclusion chromatography in S200 10/300 GL columns. A

representative size exclusion chromatogram is shown in Suppl. Figure 3B. The eight purified human anti-TIP1 full-length IgGs (L38, L111, L56, L112, L117, L127, L144, and L154) were resolved on SDS PAGE under non-reducing and reducing conditions (Suppl. Figure 4A and B). Full-length IgGs above 150 kDa were observed under non-reducing conditions (Suppl. Figure 4A). In the reducing condition, heavy and light chains were observed at 50 kDa and 25 kDa, respectively (Suppl. Figure 4B). A representative SDS-PAGE gel is shown in Figure 1F.

To select a lead anti-TIP1 human antibody for downstream applications, we evaluated the binding of the eight purified antibodies to recombinant TIP1 by ELISA, surface plasmon resonance, and cell surface binding to naturally expressed TIP1. TIP1 protein-coated microtiter plates were incubated with serial dilutions of the purified anti-TIP1 antibodies. The absorbance values were fitted using two models, one-site specific (Suppl. Figure 5A) and log (agonist) vs. response -- variable slope (four parameters) (Suppl. Figure 5B). The estimated K_d values obtained from the one site-specific binding model were 0.27±0.03, 0.12±0.01, 4.9±0.2, 0.23±0.02, 0.19±0.02, 0.17±0.03, 0.13±0.02, and 0.14±0.02 nM for antibodies L38, L111, L56, L112, L117, L127, L144, and L154 respectively. The EC50 values from the log (agonist) vs. response -- variable slope (four parameters) fitting were 0.29, 0.16, 4.7, 0.26, 0.23, 0.22, 0.17, and 0.18 nM for antibodies L38, L111, L56, L112, L117, L127, L144, and L154 respectively. The graph for L111 is shown in Figure 2A.

The equilibrium dissociation constant (K_D), association constant (K_{on}), and dissociation constant (K_{off}) of the interaction of the anti-TIP1 antibodies and recombinant TIP1 protein were evaluated using surface plasmon resonance. The overlaid sensogram of L111 is shown in Figure 2B. Supplementary table 1 shows all eight antibodies' K_D, K_{on}, and K_{off}. Rank-ordering of the eight antibodies by decreasing functional affinities shows that antibody L111 has the highest functional affinity (K_D=1.066 x 10^{-10} M) to TIP1 protein.

We evaluated the cell surface saturable binding of the eight human anti-TIP1 antibodies on H460 and A549 cells (Suppl. Figure 6). Varying concentrations of the purified antibodies were incubated with irradiated non-permeabilized H460 and A549 cells and acquired on a flow cytometer as previously described (21,22). The K_d of cell surface binding was 22.06±8.05, 5.87±1.65, 5.83±2.8, 16.65±9.7, 48.03±4.57, 12.03±4.95, 70.93±16.57, and 2.82±1.52 nM for H460 cells for antibodies L38, L111, L56, L112, L117, L127, L144, and L154 respectively (Suppl. Figure 6A). For A549 cells, the K_d values were 17.72±8.41, 0.18±0.16, 136.0±19.73, 2.32±1.2, 3.58±1.13, 5.59±3.0, 3.58±1.69, and 0.70±0.41 nM for antibodies L38, L111, L56, L112, L117, L127, L144, and L154 respectively (Suppl. Figure 6B).

Based on the ELISA, Biacore, and flow cytometry data, we selected L111 as the lead antibody for all further experiments. The lead antibody was docked with TIP1 protein *in silico* using the Schrodinger software package (Figures 2C and D). The TIP1 antibody L111's heavy chain (cyan) and light chain (magenta) are shown to interact with the TIP1 protein (green) (Figure 2C). In Figure 2D, the 3D surface model of TIP1 shows the predicted interacting residues with L111 in yellow spheres. The predicted TIP1 amino residues interacting with the antibody are D38, Q39, Q43, F46, T58, R59, V60, S61, E62,

E67, H90, D91, R94, and K95, where alphabets are single-letter amino acid codes and numbers are the position in protein sequence. These amino acids are found in the functional PDZ motif-binding pocket of TIP1. The antibody's epitope was confirmed by overlapping peptide-based epitope mapping, and a linear epitope sequence QNPFSEDKTD (N to C terminus) was identified.

In-silico immunogenicity risk assessment of L111 was performed by Lonza's Epibase platform (Figure 2E). The DRB1 score of L111 was 566.0. The score representing a low immunogenicity risk is in the range for human antibodies. The main contributors to the DRB1 score of L111 are complementarity determining region 1 (CDR 1) and framework 4 of the light chain.

Biophysical characterization of the purified human anti-TIP1 antibody L111.

The integrity of the purified L111 antibody was analyzed by non-reduced (top) and reduced (bottom) capillary electrophoresis-SDS (CE-SDS) on a Perkin Elmer LabChip GXII Touch HT (Suppl. Figure 7A). In the non-reduced CE-SDS, as expected, the dominant peak (96.72%) was the intact antibody (Suppl. Figure 7A**, top**). Under reducing conditions, we observed 75.4% of the heavy chain and 24.2% of the light chain (Suppl. Figure 7A**, bottom**). The combined light and heavy chains were 99.6%, showing the integrity of the antibody. Aggregation analysis of the purified L111 antibody was performed by size-exclusion chromatography high-performance liquid chromatography (SEC-HPLC). SEC-HPLC shows 98.37% monomers and only 1.05% of high molecular weight species (HMWS) (Suppl. Figure 7B). The charge heterogeneity profile of antibodies was characterized by cation-exchange chromatography since it potentially impacts a product's safety and efficacy. The main peak was 63.9% (Suppl. Figure 7C).

Glycosylation of anti-TIP1 antibody L111 was analyzed by native MS. Native MS was performed to evaluate the size of the purified antibody. The ESI-MS deconvoluted spectra show the size of the antibody ~146.3 kDa (Suppl. Figure 7D). Suppl. Figure 7E and F show the analysis of N-Glycan profiles and major glycan distribution of L111 antibody as determined by hydrophilic interaction liquid chromatography fluorescence detection (HILIC- FLD). FA2, FA2G1, and high-mannose 5 (M5) represent ~86% of total glycans.

L111 antibody targets human cancer cells in vitro and patient-derived xenografts in vivo

We performed flow cytometry to evaluate the cell surface binding of L111 antibody to native TIP1 on a panel of cell lines, including NSCLC (A549, H460), hepatocellular carcinoma (Hep3B, HepG2) and head and neck cancer (Cal27 and FaDu) (Figure 3A). We have previously demonstrated that TIP1 is induced on the cancer cell surface (6). Cancer cells were irradiated with three doses of 3 Gy and harvested 24 or 48 h after the last radiation dose. Figure 3A shows the bar graph of fold-change in median fluorescence intensities (MFIs) of TIP1 expression on all irradiated cancer cells compared to the sham-treatment controls. Radiation enhanced the cell surface binding of the anti-TIP1 antibody L111 compared to the sham-irradiated controls. At 24 h, the fold-change in median fluorescence intensities were 3.5±0.2 (A549, $P<0.0001$), 6.4±0.2 (H460, $P<0.0001$), 20.4±0.6 (Hep3B, $P<0.0001$), 2.2±0.1 (HepG2, $P=0.012$), 2.09±0.09 (Cal27, $P=0.032$) and 3.69±0.31 (FaDu,

P<0.0001). Similarly, at 48 h, the fold-change in median fluorescence intensities were 12.2±0.8 (A549, P<0.0001), 7.7±0.2 (H460, P<0.0001), 6.4±0.16 (Hep3B, P<0.0001), 4.0±0.2 (HepG2, P<0.0001), 3.1±0.13 (Cal27, P=0.0002) and 1.7±0.17 (FaDu, P=0.18).

The serum stability of the L111 antibody was assessed to determine whether it was stable against serum proteases. The antibody was incubated at 37° C in serum from three healthy volunteers for up to seven days, and subsequently, its binding to TIP1 was determined by ELISA assay. After seven days, the antibody was highly stable, with 90.5±6.4% of the intact antibody detected (Figure 3B).

We next performed whole-body near-infrared (NIR) imaging in NSG mice bearing a subcutaneous NSCLC patient-derived xenograft (PDX). Suppl. Figure 6C shows TIP1 immunohistochemistry in the PDX tissue used for tumor implantation. Tumors were treated with 3 Gy while shielding the rest of the mouse. The L111 and isotype control antibodies were labeled with IRDye 800 and injected into tumor-bearing mice via the tail vein. Representative NIR images from each group are shown in Figure 3C. NIR images show the binding of the L111 antibody in the PDX tumors (white arrows). Nonspecific tumor uptake of the isotype control antibody was observed, which is attributed to the enhanced permeability and retention effect. Figure 3D shows the background subtracted tumor NIR signal intensities. At 24 h, an increased mean tumor signal intensity was observed in the L111+IR (1399±61) as compared to the Anti-TIP1 Ab (580±270, P<0.0001) or Isotype+IR (876±26, P=0.0001).

Conjugation of desferoxamine to anti-TIP1 antibody L111 and its characterization

Total body imaging of cancer patients is planned to determine the optimal schedule of administration, optimal radiation regimen, and cancer subtype that is best suited to advance to phase I/II clinical trials. The positron-emitting $[^{89}Zr]Zr^{4+}$ was selected for its 78.4-hour half-life, which is well suited for whole-body imaging antibody distribution for several days. The L111 antibody was conjugated to five different molar equivalents of p-SCN-Bn-Deferoxamine (DFO) chelator using a protocol previously described (6). The molar equivalents of DFO conjugated to the L111 antibody were 1, 2, 3, 4, and 10, and the corresponding DFO-L111 antibodies were named D1, D2, D3, D4, and D10. D0 refers to the unconjugated antibody. The DFO chelator formed a stable thiourea linkage between the primary amine groups of lysine on the L111 antibody and isothiocyanate of the bifunctional chelator p-SCN-Bn-DFO (Figure 4A). The DFO-conjugated antibodies were stored at −80 °C until labeling with $[^{89}Zr]Zr^{4+}$. Native MS analysis was performed to determine the DFO to antibody ratios (DAR) for the five conjugates (Suppl. Figure 8). The average DARs were calculated to be 0.39, 0.75, 1.05, 1.34, and 3.87 for D1, D2, D3, D4, and D10 (Suppl. Table 2), respectively (Suppl. Figure 8).

We further characterized the D10-L111, which had the highest DAR of 3.87 by SEC-HPLC analysis. DFO conjugation did not change the retention time of the Ab, and no aggregation was observed (Suppl. Figure 9A). We evaluated the binding of the D10-L111 antibody to recombinant TIP1 protein by ELISA and compared it to the unconjugated antibody (Figure 4B). The ELISA data were analyzed using log (agonist) vs. response -- Variable slope (four parameters) (Figure 4B, left) and One Site – Specific binding (Figure 4B, right). The EC50

values were 0.112 nM and 0.103 nM for the unconjugated and D10-L111, respectively. The K_d values were 0.126 nM and 0.114 nM for the unconjugated and the D10-L111 antibody, respectively.

Labeling and characterization of the [^{89}Zr]Zr labeled anti-TIP1 antibody.

The D10-L111 antibody was labeled with neutralized [^{89}Zr]Zr-oxalate. The specific activity of the resulting [^{89}Zr]Zr-D10-L111 was 0.09 MBq/μg (2.5 μCi/μg) with 99.9% radiolabeling yield (Suppl. Figure 9B). Radio-HPLC confirmed the radiolabeling of the D10-L111 antibody (Suppl. Figure 9C). To evaluate the stability of DFO conjugation after freeze-thaw, we radiolabeled either freshly DFO-conjugated L111 antibody or thawed DFO-L111 Ab that was flash frozen at −80°C (Suppl. Figure 10A). The stability of both sets of [^{89}Zr]Zr-labeled antibodies was evaluated in human serum over five days. iTLC was performed to detect free [^{89}Zr]Zr^{4+}. The line graph in Suppl. Figure 10A shows 93.4% and 92.3% [^{89}Zr]Zr-labeled fresh and thawed antibodies, respectively, on day 5.

The [^{89}Zr]Zr-D10-L111 Ab was exchanged in four different buffer systems, and its stability was evaluated in human serum over seven days (Suppl. Figure 10B). After radiolabeling and buffer exchange into normal saline; 20 mM L-Histidine, 130 mM sucrose, pH 5.5; 250 mM sodium acetate, 0.5 mg/ml L-cysteine, pH 5.5; 250 mM sodium acetate, 5 mg/ml Gentisic acid, pH 5.5, [^{89}Zr]Zr-D10-L111 Ab was incubated in human serum and evaluated over seven days by iTLC (Suppl. Figure 10B). After seven days, 99.89%, and 98.08% intact [^{89}Zr]Zr-D10-L111 Ab in normal saline and 20 mM L-Histidine, 130 mM sucrose, pH 5.5 buffers, respectively. In contrast, there was only 65.20% and 46.74% intact [^{89}Zr]Zr-L111 Ab in 250 mM sodium acetate, 5 mg/ml Gentisic acid, pH 5.5, and 250 mM sodium acetate, 0.5 mg/ml L-cysteine, pH 5.5 buffers respectively. We, therefore, used normal saline for all studies with the [^{89}Zr]Zr-labeled L111 Ab.

The binding specificity of [^{89}Zr]Zr-D10-L111 Ab to cell surface TIP1 was examined *in vitro* in A549 and H460 cells. With the competitive blocking by non-radiolabeled L111, the binding of [^{89}Zr]Zr-D10-L111 Ab to A549 ($P<0.0001$) and H460 ($P<0.0001$) cells was significantly reduced (Figure 4C). We evaluated the internalization of the [^{89}Zr]Zr-D10-L111 Ab in A549 cells. After 24 h, 57% of the antibody was internalized, and 42.9% was bound on the cell surface. After five days, 75.7% internalization was observed (Figure 4D).

Small animal PET imaging and biodistribution with [^{89}Zr]Zr-DFO-L111

We studied the biodistribution of [^{89}Zr]Zr-D10-L111 and [^{89}Zr]Zr-D10-Isotype control antibody in nude mice bearing A549 tumors in the hind limb (Suppl. Figure 11). A549 tumors were irradiated with three doses of 3 Gy over 24 h, followed by injection with radiolabeled antibodies and organ harvesting at days 2 and 5 post-injection. 40 mg/kg cold Ab was injected before the radiolabeled was injected for the tumor-blocking study. On both days a significantly ($P<0.01$) higher uptake of [^{89}Zr]Zr-D10-L111 (8.9±0.3 %ID/g on day 2; 7.4±0.8 %ID/g on day 5) was observed in the tumors compared to the [^{89}Zr]Zr-D10-isotype control (5.5±0.4 %ID/g on day 2; 4.8±0.7 %ID/g on day 5). Preinjection with 40 mg/kg cold

L111 significantly blocked the uptake of [^{89}Zr]Zr-D10-L111 in tumors (4.5±0.8 %ID/g) ($P<0.05$).

We wanted to optimize the tumor uptake of [^{89}Zr]Zr-DFO-L111 further. We hypothesized that the high DAR (3.87) of the D10 may impair the target binding *in vivo*. Affinity analysis by surface plasmon resonance (SPR) showed a nine-fold decrease in the binding affinity of the D10 conjugate, whereas a five-fold decrease was observed in the D3 conjugate (Suppl. Table 3). In fact, when we compared the cell surface immunoreactivity of the radiolabeled DAR 3.87 vs. DAR 1.05 antibodies, we found 81% vs. 96% immunoreactive fractions, respectively (Figure 5A). We also evaluated whether the radiolabeling of the D3 conjugate affects the antibody integrity by SDS-PAGE and autoradiography (Suppl. Figure 12A). An intact antibody was observed at 150kDa under non-reducing conditions, and both heavy and light chains of the IgG were visible under non-reducing conditions. In the ELISA assay, the radiolabeled D3 maintained antigen binding as compared to the unconjugated L111 or DFO-L111 (Suppl. Figure 12B). Therefore, the [^{89}Zr]Zr-D3-L111 was evaluated by small animal PET imaging and post-PET biodistribution measurements in A549 and H460 tumor-bearing mice. The [^{89}Zr]Zr-D3-L111 will be denoted as [^{89}Zr]Zr-DFO-L111 from here onwards.

Previous PET studies of trastuzumab utilized the injection of cold trastuzumab prior to [^{89}Zr]Zr-Trastuzumab for enhanced signal/noise visualization in tumors since the cold trastuzumab reduced uptake in normal organs (23-25). To determine the optimum dose of the cold L111 for normal tissue blocking and enhanced tumor uptake, we performed near-infrared (NIR) imaging of organs harvested from A549 and H460 tumor-bearing mice (Figure 5B and C). We injected 0, 0.4, 4, and 40 mg/kg unlabeled L111 antibodies prior to IRDye800 labeled L111. Murine organs were harvested, and their NIR signal intensity per gm was plotted (Figure 5B and C). In both A549 ($P<0.05$) and H460 ($P<0.01$) tumor models, a significantly higher tumor uptake of the IRDye800 labeled L111 was observed when the mice were pre-injected with 4 mg/kg unlabeled L111 compared to no unlabeled L111 preinjection. Moreover, there was no difference in tumor uptake of the L111 antibody based on the time interval between preinjection of the unlabeled antibody and IRDye800 labeled L111.

We performed small animal PET imaging and post-PET biodistribution (Figure 6) with the [^{89}Zr]Zr-DFO-L111 in A549 and H460 tumor models. The tumor implantation and treatment schema are shown in Suppl. Figure 13A. For normal tissue blocking and enhanced signal-to-noise tumor visualization, mice were injected with 4 mg/kg cold L111 before [^{89}Zr]Zr-DFO-L111. Figures 6A and B show representative images on days 2 and 5 post-injection for H460 and A549 tumor-bearing mice, respectively. On visual inspection of the PET images, we found enhanced tumor uptake and reduced normal tissue uptake of [^{89}Zr]Zr-DFO-L111 in mice injected with 4 mg/kg cold L111 prior to [^{89}Zr]Zr-DFO-L111 as compared to the mice that were injected with only [^{89}Zr]Zr-DFO-L111 (Figure 6A and B). The tumor-to-muscle SUVmax ratios significantly increased ($P<0.0001$) from 8.04±0.5 on day 2 to 15.65±1.9 on day 5 in H460 mice injected with cold L111 prior to [^{89}Zr]Zr-DFO-L111 (Figure 6C). Post-PET biodistribution was performed on day 5. The liver uptake in H460 tumor-bearing mice injected with 4 mg/kg cold L111 prior to [^{89}Zr]Zr-DFO-L111

(8.4±1.3% ID/g) was lower than in mice injected with only [^{89}Zr]Zr-DFO-L111 (12.6±2.4 % ID/g) (Figure 6D). The H460 tumor uptake of the radiolabeled antibody was higher (12.15±0.6% ID/g) in mice injected with 4 mg/kg cold L111 prior to [^{89}Zr]Zr-DFO-L111 than in mice only injected with the [^{89}Zr]Zr-DFO-L111 (10.09±2.7 % ID/g) (Figure 6D). The uptake in the spleen was similar in both groups.

Similarly, the tumor-to-muscle SUVmax ratios significantly increased ($P<0.05$) from 6.2±0.5 on day 2 to 9.8±2.0 on day 5 in A549 mice injected with cold L111 prior to [^{89}Zr]Zr-DFO-L111 (Figure 6E). The tumor SUVmax at days 2 and 5 for H460 and A549 tumors are shown in Suppl. Figure 13B and C, respectively. The liver uptake in A549 tumor-bearing mice injected with 4 mg/kg cold L111 prior to [^{89}Zr]Zr-DFO-L111 (7.0±0.7 % ID/g) was lower than in mice only injected with the [^{89}Zr]Zr-DFO-L111 (8.9±0.7 % ID/g) (Figure 6F). The A549 tumor uptake of the radiolabeled antibody was higher (9.1±1.2 % ID/g) in mice injected with 4 mg/kg cold L111 prior to [^{89}Zr]Zr-DFO-L111 than in mice only injected with the [^{89}Zr]Zr-DFO-L111 (7.8±1.8 % ID/g) (Figure 6F).

Discussion

Targeted drug delivery to cancer can be achieved through the exploitation of inducible antigens that translocate to the cancer cell surface in response to cytotoxic therapy. We have shown that radiosensitizing drugs like MMAE can enhance the efficacy of radiotherapy when conjugated with an anti-TIP1 antibody (6). In the present studies, we optimized the manufacturing, chemistry, and controls of the human anti-TIP1 antibody, L111, which will be studied in cancer patients. scFv phage display of human antibodies is a versatile, reproducible, and functional technology that can be utilized to isolate high-affinity antibody candidates. There are 14 phage-display-derived antibodies approved by the FDA (26). We created the scFv phage display library (WashU-II) from non-immune healthy donors' blood. Previous studies have reported scFv libraries created from spleens (15) and lymph nodes (16). Following three rounds of biopanning the WashU-II phage-displayed library against the recombinant TIP1 protein, we isolated several scFvs, eight of which were used to create human IgG1 antibodies.

Antibody engineering technologies allow for the reformatting of scFvs to full-length IgGs (13,14). We reformatted the eight scFvs to full-length human IgG1 antibodies and expressed them in suspension ExpiCHO-S™ Cells. Mammalian expression systems can produce fully glycosylated recombinant antibodies (13,14). The purified antibodies (150 kDa) were evaluated for their functional affinities to recombinant TIP1 protein by ELISA and surface plasmon resonance assays. Seven antibodies had subnanomolar affinities to TIP1, the highest of 1.06×10^{-10} M for the L111 antibody. Flow cytometry was performed to evaluate the binding of all antibodies to cell surface TIP1. Saturable cell surface binding was observed for all antibodies except L56 Ab. The L111 Ab was selected for further evaluation because of its high-affinity binding to recombinant and cell surface-expressed TIP1.

Computational docking is an emerging technique that allows the prediction of the conformation of the complex from its components (27). In our docking studies, we used

the crystal structure of TIP1 (3DIW) and docked it to the model of L111 Ab. The predicted TIP1 amino residues interacting with the antibody were found in the functional PDZ motif-binding pocket of TIP1. The interacting residues were confirmed by epitope mapping using overlapping peptides, and the peptide sequence QNPFSEDKTD (N to C terminus) was identified.

It is critical to study the integrity and stability of monoclonal antibodies, which can easily undergo fragmentation during the production and purification phase (28). Cleavage of the hinge polypeptide is a well-known fragmentation process that occurs via hydrolysis or β-elimination as a function of the amino acid sequence, pH, temperature, and formulation buffer (29-31). Fragmentation may negatively impact the safety and efficacy of the monoclonal antibodies. We performed the biophysical characterization of the purified L111 Ab by CE-SDS, SEC-HPLC, and cation-exchange chromatography. CE-SDS offers many advantages over the traditional SDS-PAGE gel technology with respect to speed and resolution (32). As expected, the purified L111 Ab was intact under non-reducing conditions (96.72% dominant peak), and the combined light and heavy chain was 99.6% under reducing conditions.

Antibody aggregation is undesirable because it can compromise biological functions (33), induce immune responses (34), and activate antibody clearance machinery *in vivo* (35). Size-exclusion chromatography (SEC) is used for the quantitative assessment of antibody aggregation (including dimers and multimers) because of its speed and reproducibility. SEC-HPLC of the lead anti-TIP1 antibody L111 shows a desirable profile of 98.37% monomer species.

Glycosylation is a post-translational modification that occurs during the production of antibodies. Glycans attached to antibodies play an important role in the pharmacokinetics, efficacy, and safety of therapeutic antibodies (36,37). We found FA2, FA2G1, and high-mannose 5 (M5) representing 86% of total glycans in the L111 Ab. This glycan profile is commonly found in the recombinant antibodies produced from CHO cells (38).

Once injected into humans, antibodies need to remain intact and active for days at 37 °C in human plasma in order to accumulate at the specific target site in the tumor tissue. The antibodies should not precipitate, degrade, or undergo inactivation. Antibody stability can be measured *in vitro* in human serum by indirect ELISA to detect antigen binding. We found that the unconjugated anti-TIP1 antibody L111 was highly stable (90.5±6.4% of the immunoreactive antibody) after seven days in human serum.

We have previously demonstrated that TIP1 expression is induced on the cancer cell surface (6). We evaluated the cell surface binding of the lead anti-TIP1 antibody to a panel of cancer cell lines following irradiation. Enhanced binding of the antibody was observed on all cell lines following irradiation. Similarly, in PDX tumors implanted in NSG mice, we found a significantly higher ($p<0.0001$) uptake of the anti-TIP1 antibody following tumor irradiation compared to unirradiated tumors. In the irradiation groups, the anti-TIP1 antibody uptake was significantly higher ($P=0.001$) compared to the isotype control. Nonspecific tumor

uptake of the isotype control antibody was observed, which is attributed to the enhanced permeability and retention effect.

We developed the L111 antibody for noninvasive imaging of cancer patients. The positron emitter [^{89}Zr]Zr is well suited for antibody-based PET imaging (immuno-PET) since it has a half-life of 78.4 h, which matches the pharmacokinetics of antibodies, and it has a low average positron energy of 395 keV, making it an ideal candidate for high-resolution PET imaging of slow-accumulating biomolecules (10). DFO is most widely used for the chelation of [^{89}Zr]Zr to antibodies (20,39). Since DFO linkage involves the free primary amine groups of lysine on the anti-TIP1 antibody, we evaluated five different molar equivalents (1, 2, 3, 4, and 10) of DFO conjugated to the L111. The corresponding DFO-L111 antibodies were named D1, D2, D3, D4 and D10 respectively. The average degree of DFO conjugation to L111 antibody (DAR) was determined via native MS using the unmodified L111 as the reference. As expected, the degree of DFO conjugation increased with the increasing molar equivalents. The average DARs were 0.39, 0.75, 1.05, 1.34, and 3.87 for D1, D2, D3, D4, and D10, respectively. Since previous studies with DFO-conjugated antibodies reported average DARs of ~3 or more (40-42), we performed further studies with the D10 conjugate.

We characterized the D10 L111 DFO-conjugated antibody for aggregation and antigen binding. No aggregation of the D10 antibody was found in SEC-HPLC. In ELISA antigen binding assays, the Kd of the D10 antibody was 0.114 nM compared to 0.126 nM for the unconjugated L111 antibody. The D10 antibody was labeled with [^{89}Zr]Zr with 99.9% radiolabeling yield. After radiolabeling, the D10 antibody was buffer exchanged into four different buffers, including normal saline, histidine-sucrose buffer, sodium acetate containing L-cysteine, and sodium acetate containing gentisic acid and its stability evaluated in human serum *in vitro.* After seven days, 99.89% intact [^{89}Zr]Zr-D10-L111 Ab was found in normal saline, and therefore this buffer was used in all studies. The DFO conjugation to the anti-TIP1 antibody was stable to freeze-thaw, as demonstrated by highly stable radiolabeled antibodies in human serum *in vitro*.

[^{89}Zr]Zr-D10-L111 Ab demonstrated high-affinity binding to the cell surface of A549 and H460 cells. Competitive blocking with cold L111 significantly blocked ($P<0.0001$) cell surface binding of the [^{89}Zr]Zr-D10-L111 Ab. We have previously reported the internalization of cell surface TIP1 following antibody binding. We exploited the endocytosis induction for the delivery of a radiation-sensitizing drug (6). Labeling of the lead anti-TIP1 antibody with [^{89}Zr]Zr did not attenuate its endocytosis. After five days, 75.7% of the L111 antibody was internalized. In biodistribution studies, we found a significantly higher tumor uptake ($P=0.01$) of the [^{89}Zr]Zr-D10-L111 Ab compared to the isotype control. Preinjection of the 40 mg/kg cold antibody blocked the uptake of the [^{89}Zr]Zr-D10-L111 Ab in the irradiated tumors, indicating specific tumor binding.

We hypothesized that the high DAR 3.87 might hamper target binding *in vivo.* On comparing the affinities of the DAR 1.05 to that of DAR 3.87 by surface plasmon resonance (SPR), we found a nine-fold decrease in the binding affinity of the DAR 3.87 conjugate, and a five-fold decrease was observed in the DAR 1.05 conjugate. This difference in affinity was not evident in the ELISA assay due to its lower sensitivity

compared to SPR. The radiolabeling efficiency of both D3 and D10 was 99.9%. In the cell surface immunoreactivity assay, we found a higher immunoreactive fraction (96%) with the [^{89}Zr]Zr-D3-L111 Ab compared to the [^{89}Zr]Zr-D10-L111 Ab (81%). The affinity and immunoreactivity data suggest that a DAR of ~1, as found in the D3, is optimal for the L111 antibody labeling with [^{89}Zr]Zr. A similar finding was that more than three chelators per trastuzumab antibody had a decreased *in vivo* performance (39).

We performed small animal PET imaging and post-PET biodistribution with the [^{89}Zr]Zr-D3-L111 in the H460 and A549 tumor models. Earlier studies found that injecting unconjugated antibodies before radiolabeled antibodies enhances tumor signals by reducing nonspecific binding to normal tissues (23-25). To employ this concept in our studies with the [^{89}Zr]Zr-D3-L111 Ab, we first evaluated a range of doses (0, 0.4, 4, and 40 mg/kg) of unlabeled L111 injection prior to NIR dye-labeled L111 injection into H460 and A549 tumor-bearing mice. The organ signal intensity per gm indicated the highest tumor binding in the group injected with 4 mg/kg unlabeled L111. Therefore, a 4 mg/kg dose of cold L111 was used to enhance the signal-to-noise ratio in small animal PET imaging studies with [^{89}Zr]Zr-DFO-L111. In PET, we found a significant increase ($P<0.01$) in the tumor-to-muscle SUVmax ratios from days 2 to 5 post-radiolabeled antibody injection in both A549 and H460 tumor models. The post-PET biodistribution study also revealed a lower liver signal in the mice that had 4 mg/kg cold antibody injected prior to [^{89}Zr]Zr-DFO-L111.

Overall, we developed a novel human antibody that can target inducible cell surface TIP1. Whole-body PET imaging of the [^{89}Zr]Zr-DFO-L111 will be used to determine the optimal schedule of administration, optimal radiation regimen, and cancer subtype that is best suited to advance to phase I/II clinical trials of the anti-TIP1 antibody. During planned therapy studies, the L111 antibody will be conjugated to therapeutic radioisotopes like ^{90}Y, ^{225}Ac or to radiosensitizing drugs like MMAE and SN38. The radioimmunoconjugate or the antibody-drug conjugates will be used to treat patients whose tumors show enhanced TIP1 expression after radiation.

Supplementary Material

Refer to Web version on PubMed Central for supplementary material.

Acknowledgments:

This study was supported by NIH R44CA210687 (D. Hallahan), Siteman Cancer Center, and Elizabeth and James McDonnell endowment (D. Hallahan). This work was performed with support from the Siteman Cancer Center Small Animal Imaging Core. This study made use of the Washington University Biomedical Mass Spectrometry Resource and the Mass Spectrometry Technology Access Center at the McDonnell Genome Institute (MTAC@MGI) at Washington University School of Medicine. We thank Nikki Fettig, Margaret Morris, and Amanda Klaas for their technical support with the tail vein injections, small animal PET imaging, and biodistribution studies.

References

1. Mueller AC, Piper M, Goodspeed A, Bhuvane S, Williams JS, Bhatia S, et al. Induction of ADAM10 by Radiation Therapy Drives Fibrosis, Resistance, and Epithelial-to-Mesenchyal Transition in Pancreatic Cancer. Cancer Res 2021;81(12):3255–69 doi 10.1158/0008-5472.CAN-20-3892. [PubMed: 33526513]

2. Dadey DYA, Kapoor V, Khudanyan A, Thotala D, Hallahan DE. PERK Regulates Glioblastoma Sensitivity to ER Stress Although Promoting Radiation Resistance. Mol Cancer Res 2018;16(10):1447–53 doi 10.1158/1541-7786.MCR-18-0224. [PubMed: 29991528]

3. Dadey DY, Kapoor V, Khudanyan A, Urano F, Kim AH, Thotala D, et al. The ATF6 pathway of the ER stress response contributes to enhanced viability in glioblastoma. Oncotarget 2016;7(2):2080–92 doi 10.18632/oncotarget.6712. [PubMed: 26716508]

4. Singh AK, Dadey DY, Rau MJ, Fitzpatrick J, Shah HK, Saikia M, et al. Blocking the functional domain of TIP1 by antibodies sensitizes cancer to radiation therapy. Biomed Pharmacother 2023;166:115341 doi 10.1016/j.biopha.2023.115341. [PubMed: 37625322]

5. Kapoor V, Singh AK, Lewis CD, Deore S, Hallahan DE. Exploiting Radiation Induction of Antigens in Cancer: Targeted Drug Delivery. Int J Mol Sci 2022;23(6) doi 10.3390/ijms23063041.

6. Lewis CD, Singh AK, Hsu FF, Thotala D, Hallahan DE, Kapoor V. Targeting a Radiosensitizing Antibody-Drug Conjugate to a Radiation-Inducible Antigen. Clin Cancer Res 2021;27(11):3224–33 doi 10.1158/1078-0432.CCR-20-1725. [PubMed: 34074654]

7. Kapoor V, Singh AK, Rogers BE, Thotala D, Hallahan DE. PEGylated peptide to TIP1 is a novel targeting agent that binds specifically to various cancers in vivo. J Control Release 2019;298:194–201 doi 10.1016/j.jconrel.2019.02.008. [PubMed: 30763622]

8. Yan H, Kapoor V, Nguyen K, Akers WJ, Li H, Scott J, et al. Anti-tax interacting protein-1 (TIP-1) monoclonal antibody targets human cancers. Oncotarget 2016;7(28):43352–62 doi 10.18632/oncotarget.9713. [PubMed: 27270318]

9. Mohanty S, Ovee M, Banerjee M. PDZ Domain Recognition: Insight from Human Tax-Interacting Protein 1 (TIP-1) Interaction with Target Proteins. Biology (Basel) 2015;4(1):88–103 doi 10.3390/biology4010088. [PubMed: 25665168]

10. Yoon JK, Park BN, Ryu EK, An YS, Lee SJ. Current Perspectives on (89)Zr-PET Imaging. Int J Mol Sci 2020;21(12) doi 10.3390/ijms21124309.

11. Manafi-Farid R, Ataeinia B, Ranjbar S, Jamshidi Araghi Z, Moradi MM, Pirich C, et al. ImmunoPET: Antibody-Based PET Imaging in Solid Tumors. Front Med (Lausanne) 2022;9:916693 doi 10.3389/fmed.2022.916693. [PubMed: 35836956]

12. Hegi-Johnson F, Rudd S, Hicks RJ, De Ruysscher D, Trapani JA, John T, et al. Imaging immunity in patients with cancer using positron emission tomography. NPJ Precis Oncol 2022;6(1):24 doi 10.1038/s41698-022-00263-x. [PubMed: 35393508]

13. Vazquez-Lombardi R, Nevoltris D, Luthra A, Schofield P, Zimmermann C, Christ D. Transient expression of human antibodies in mammalian cells. Nat Protoc 2018;13(1):99–117 doi 10.1038/nprot.2017.126. [PubMed: 29240734]

14. Wurm FM. Production of recombinant protein therapeutics in cultivated mammalian cells. Nat Biotechnol 2004;22(11):1393–8 doi 10.1038/nbt1026. [PubMed: 15529164]

15. Diebolder P, Mpoy C, Scott J, Huynh TT, Fields R, Spitzer D, et al. Preclinical Evaluation of an Engineered Single-Chain Fragment Variable-Fragment Crystallizable Targeting Human CD44. J Nucl Med 2021;62(1):137–43 doi 10.2967/jnumed.120.249557. [PubMed: 32513906]

16. Diebolder P, Keller A, Haase S, Schlegelmilch A, Kiefer JD, Karimi T, et al. Generation of "LYmph Node Derived Antibody Libraries" (LYNDAL) for selecting fully human antibody fragments with therapeutic potential. MAbs 2014;6(1):130–42 doi 10.4161/mabs.27236. [PubMed: 24256717]

17. Kapoor V, Singh AK, Dey S, Sharma SC, Das SN. Circulating cycloxygenase-2 in patients with tobacco-related intraoral squamous cell carcinoma and evaluation of its peptide inhibitors as potential antitumor agent. Journal of cancer research and clinical oncology 2010;136(12):1795–804 doi 10.1007/s00432-010-0837-4. [PubMed: 20213098]

18. Singh AK, Singh R, Naz F, Chauhan SS, Dinda A, Shukla AA, et al. Structure based design and synthesis of peptide inhibitor of human LOX-12: in vitro and in vivo analysis of a novel therapeutic agent for breast cancer. PLoS One 2012;7(2):e32521 doi 10.1371/journal.pone.0032521. [PubMed: 22384268]

19. Kapoor V, Dadey DY, Nguyen K, Wildman SA, Hoye K, Khudanyan A, et al. Tumor-Specific Binding of Radiolabeled PEGylated GIRLRG Peptide: A Novel Agent for Targeting Cancers. J Nucl Med 2016;57(12):1991–7 doi 10.2967/jnumed.115.165118. [PubMed: 27445290]

20. Vosjan MJ, Perk LR, Visser GW, Budde M, Jurek P, Kiefer GE, et al. Conjugation and radiolabeling of monoclonal antibodies with zirconium-89 for PET imaging using the bifunctional chelate p-isothiocyanatobenzyl-desferrioxamine. Nat Protoc 2010;5(4):739–43 doi 10.1038/nprot.2010.13. [PubMed: 20360768]
21. Yang Z, Wan Y, Tao P, Qiang M, Dong X, Lin CW, et al. A cell-cell interaction format for selection of high-affinity antibodies to membrane proteins. Proc Natl Acad Sci U S A 2019;116(30):14971–8 doi 10.1073/pnas.1908571116. [PubMed: 31285332]
22. Frank GM, Angeletti D, Ince WL, Gibbs JS, Khurana S, Wheatley AK, et al. A Simple Flow-Cytometric Method Measuring B Cell Surface Immunoglobulin Avidity Enables Characterization of Affinity Maturation to Influenza A Virus. mBio 2015;6(4):e01156 doi 10.1128/mBio.01156-15. [PubMed: 26242629]
23. Dijkers EC, Oude Munnink TH, Kosterink JG, Brouwers AH, Jager PL, de Jong JR, et al. Biodistribution of 89Zr-trastuzumab and PET imaging of HER2-positive lesions in patients with metastatic breast cancer. Clin Pharmacol Ther 2010;87(5):586–92 doi 10.1038/clpt.2010.12. [PubMed: 20357763]
24. Laforest R, Lapi SE, Oyama R, Bose R, Tabchy A, Marquez-Nostra BV, et al. [(89)Zr]Trastuzumab: Evaluation of Radiation Dosimetry, Safety, and Optimal Imaging Parameters in Women with HER2-Positive Breast Cancer. Mol Imaging Biol 2016;18(6):952–9 doi 10.1007/s11307-016-0951-z. [PubMed: 27146421]
25. Dehdashti F, Wu N, Bose R, Naughton MJ, Ma CX, Marquez-Nostra BV, et al. Evaluation of [(89)Zr]trastuzumab-PET/CT in differentiating HER2-positive from HER2-negative breast cancer. Breast Cancer Res Treat 2018;169(3):523–30 doi 10.1007/s10549-018-4696-z. [PubMed: 29442264]
26. Alfaleh MA, Alsaab HO, Mahmoud AB, Alkayyal AA, Jones ML, Mahler SM, et al. Phage Display Derived Monoclonal Antibodies: From Bench to Bedside. Front Immunol 2020;11:1986 doi 10.3389/fimmu.2020.01986. [PubMed: 32983137]
27. Pedotti M, Simonelli L, Livoti E, Varani L. Computational docking of antibody-antigen complexes, opportunities and pitfalls illustrated by influenza hemagglutinin. Int J Mol Sci 2011;12(1):226–51 doi 10.3390/ijms12010226. [PubMed: 21339984]
28. Vlasak J, Ionescu R. Fragmentation of monoclonal antibodies. MAbs 2011;3(3):253–63 doi 10.4161/mabs.3.3.15608. [PubMed: 21487244]
29. Xiao G, Bondarenko PV. Identification and quantification of degradations in the Asp-Asp motifs of a recombinant monoclonal antibody. J Pharm Biomed Anal 2008;47(1):23–30 doi 10.1016/j.jpba.2007.11.050. [PubMed: 18201853]
30. Ishikawa T, Ito T, Endo R, Nakagawa K, Sawa E, Wakamatsu K. Influence of pH on heat-induced aggregation and degradation of therapeutic monoclonal antibodies. Biol Pharm Bull 2010;33(8):1413–7 doi 10.1248/bpb.33.1413. [PubMed: 20686240]
31. Salinas BA, Sathish HA, Shah AU, Carpenter JF, Randolph TW. Buffer-dependent fragmentation of a humanized full-length monoclonal antibody. J Pharm Sci 2010;99(7):2962–74 doi 10.1002/jps.22056. [PubMed: 20091831]
32. Rustandi RR, Wang Y. Use of CE-SDS gel for characterization of monoclonal antibody hinge region clipping due to copper and high pH stress. Electrophoresis 2011;32(21):3078–84 doi 10.1002/elps.201100186. [PubMed: 22145164]
33. Lowe D, Dudgeon K, Rouet R, Schofield P, Jermutus L, Christ D. Aggregation, stability, and formulation of human antibody therapeutics. Adv Protein Chem Struct Biol 2011;84:41–61 doi 10.1016/B978-0-12-386483-3.00004-5. [PubMed: 21846562]
34. De Groot AS, Scott DW. Immunogenicity of protein therapeutics. Trends Immunol 2007;28(11):482–90 doi 10.1016/j.it.2007.07.011. [PubMed: 17964218]
35. Hotzel I, Theil FP, Bernstein LJ, Prabhu S, Deng R, Quintana L, et al. A strategy for risk mitigation of antibodies with fast clearance. MAbs 2012;4(6):753–60 doi 10.4161/mabs.22189. [PubMed: 23778268]
36. Jefferis R. Glycosylation as a strategy to improve antibody-based therapeutics. Nat Rev Drug Discov 2009;8(3):226–34 doi 10.1038/nrd2804. [PubMed: 19247305]

37. Wada R, Matsui M, Kawasaki N. Influence of N-glycosylation on effector functions and thermal stability of glycoengineered IgG1 monoclonal antibody with homogeneous glycoforms. MAbs 2019;11(2):350–72 doi 10.1080/19420862.2018.1551044. [PubMed: 30466347]

38. Trappe A, Fussl F, Millan-Martin S, Ronan R, Zaborowska I, Bones J. Correlative N-glycan and charge variant analysis of cetuximab expressed in murine, chinese hamster and human expression systems. J Chromatogr B Analyt Technol Biomed Life Sci 2022;1194:123186 doi 10.1016/j.jchromb.2022.123186.

39. Sharma SK, Glaser JM, Edwards KJ, Khozeimeh Sarbisheh E, Salih AK, Lewis JS, et al. A Systematic Evaluation of Antibody Modification and (89)Zr-Radiolabeling for Optimized Immuno-PET. Bioconjug Chem 2021;32(7):1177–91 doi 10.1021/acs.bioconjchem.0c00087. [PubMed: 32197571]

40. Raave R, Sandker G, Adumeau P, Jacobsen CB, Mangin F, Meyer M, et al. Direct comparison of the in vitro and in vivo stability of DFO, DFO* and DFOcyclo* for (89)Zr-immunoPET. Eur J Nucl Med Mol Imaging 2019;46(9):1966–77 doi 10.1007/s00259-019-04343-2. [PubMed: 31161258]

41. Ghai A, Maji D, Cho N, Chanswangphuwana C, Rettig M, Shen D, et al. Preclinical Development of CD38-Targeted [(89)Zr]Zr-DFO-Daratumumab for Imaging Multiple Myeloma. J Nucl Med 2018;59(2):216–22 doi 10.2967/jnumed.117.196063. [PubMed: 29025987]

42. Ghai A, Zheleznyak A, Mixdorf M, O'Neal J, Ritchey J, Rettig M, et al. Development of [(89)Zr]DFO-elotuzumab for immunoPET imaging of CS1 in multiple myeloma. Eur J Nucl Med Mol Imaging 2021;48(5):1302–11 doi 10.1007/s00259-020-05097-y. [PubMed: 33179150]

Translational Relevance

TIP1 is overexpressed in cancers, including lung, breast, and gliomas, and mediates cancer progression and resistance to therapy. It translocates to the cancer cell surface in response to radiation. We developed the human anti-TIP1 antibody, L111, for noninvasive imaging of cancer patients. L111 was selected by biopanning an in-house phage-displayed scFv library created from the blood of healthy donors. The scFv was engineered to a human IgG1 and labeled with the positron emitter [^{89}Zr]Zr. We demonstrated specific radiation-guided tumor targeting of the radiolabeled antibody in preclinical models. Whole-body PET imaging of the [^{89}Zr]Zr-DFO-L111 will be used to determine the optimal schedule of administration, optimal radiation regimen, and cancer subtype that is best suited to advance to phase I/II clinical trials of the anti-TIP1 antibody.

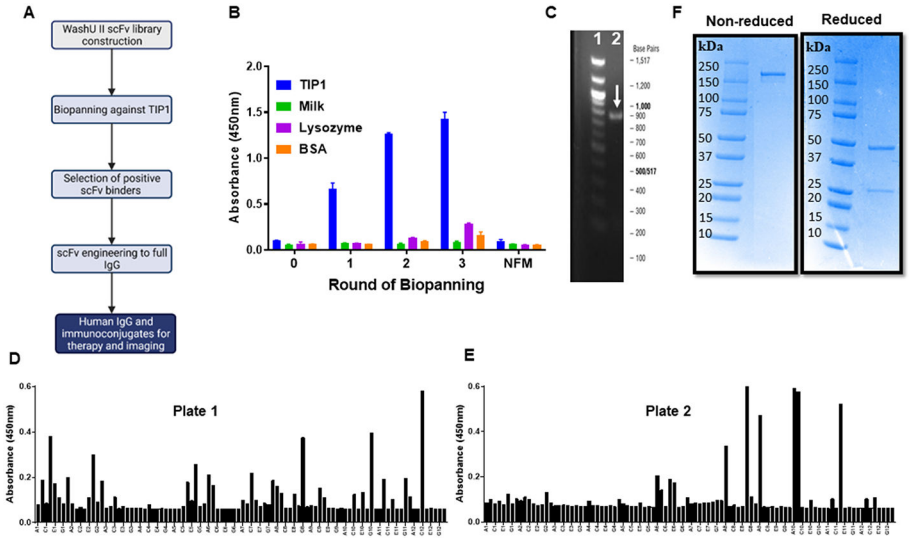

Figure 1. Anti-TIP1 human scFv discovery and engineering to a full-length IgG.

A. Schematic representation of the steps for antibody discovery and engineering using the WashU II phage-display library. **B.** Bar graph of polyclonal phage ELISA showing enrichment of TIP1 specific scFvs with three rounds of biopanning. The ELISA plates were coated with TIP1, Milk, lysozyme, or BSA and probed with phages eluted from three rounds of biopanning with the recombinant TIP1 protein. NFM: Non-fat milk. **C.** Representative DNA gel showing the amplification of a full-length scFv from the phagemid. Lane 1 represents the 100 bp DNA ladder with the indicated base pairs outside the gel image. Lane 2 is the amplified scFv indicated with a white arrow. **D** and **E.** Two different 96-well plates of monoclonal phage ELISA showing positive anti-TIP1 scFv binders. The ELISA plates were coated with recombinant TIP1 protein and probed with monoclonal phages obtained after the three rounds of biopanning. Each bar represents a single phage clone. **F.** Purified human L111 antibody was resolved on SDS-PAGE under non-reducing and reducing conditions. L111 is observed above 150 kDa under non-reducing conditions. Heavy and light chains are observed in the reducing condition at 50 kDa and 25 kDa, respectively.

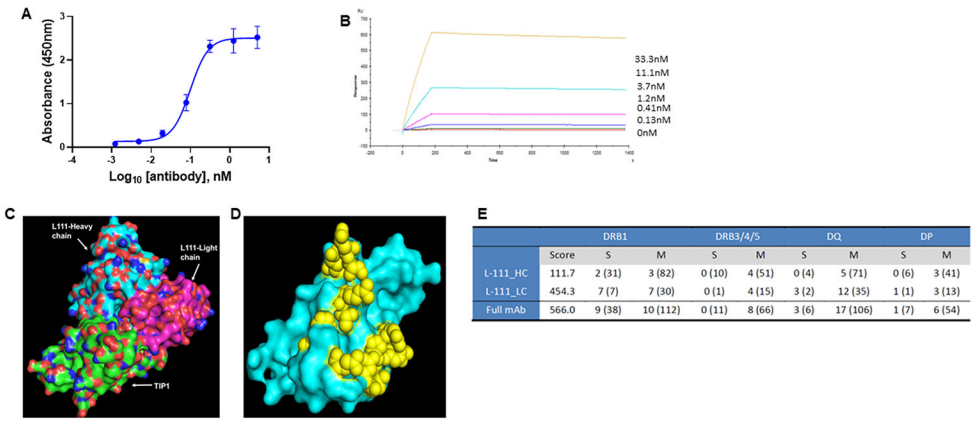

	DRB1			DRB3/4/5		DQ		DP	
	Score	S	M	S	M	S	M	S	M
L-111_HC	111.7	2 (31)	3 (82)	0 (10)	4 (51)	0 (4)	5 (71)	0 (6)	3 (41)
L-111_LC	454.3	7 (7)	7 (30)	0 (1)	4 (15)	3 (2)	12 (35)	1 (1)	3 (13)
Full mAb	566.0	9 (38)	10 (112)	0 (11)	8 (66)	3 (6)	17 (106)	1 (7)	6 (54)

Figure 2. Binding of L111 antibody to the TIP1 protein.

A. ELISA assay for the binding of L111 antibody to recombinant TIP1 protein. TIP1 protein was coated on ELISA plates. Four-fold serial dilutions (starting at 5 nM) of the purified L111 antibodies were incubated with the protein. Anti-human HRP conjugated antibody was used as the detection antibody along with TMB substrate. Absorbance at 450 nm vs. concentration is plotted in the graph. The data were fitted using the log (agonist) vs. response -- Variable slope (four parameters) model in GraphPad Prism software. **B.** Recombinant TIP1 protein (ligand) was immobilized on the surface of the CM5 sensor chip. The reference surface was prepared and blocked. Various concentrations of L111 antibodies (as indicated) were passed over the ligand. Reference subtracted sensograms were fitted using the BIAevaluation software, and on-rates, off-rates, and K_D were calculated. **C.** Computational docking of TIP1 with L111 antibody was performed using the Schrodinger software package. The L111 antibody heavy chain (cyan) and light chain (magenta) are shown to interact with the TIP1 protein (green). **D.** The 3D surface model of TIP1 shows the predicted interacting residues with the L111 antibody in yellow spheres. **E**. Immunogenicity assessment of L111 antibody. The table shows DRB1 scores and epitope counts per gene family and per binding strength class. Numbers in brackets refer to TCR-filtered and self-peptides.

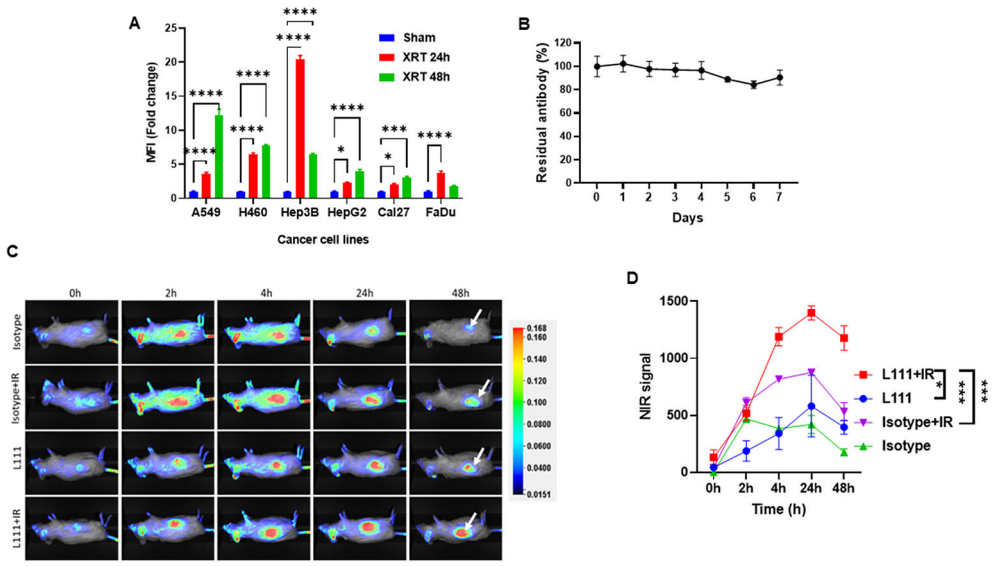

Figure 3. L111 antibody targets human cancer cells *in vitro* and patient-derived xenografts *in vivo*.

A. Bar graph showing the fold-change in median fluorescence intensities representing the binding of the L111 antibody on the surface of cancer cells. Lung cancer (A549 and H460), liver cancer (Hep3B and HepG2), and head and neck cancer (Cal27 and FaDu) cells were either sham-irradiated or irradiated with three doses of 3 Gy radiation. Cells were harvested 24 or 48 h post irradiation, and the surface binding of L111 was evaluated by flow cytometry. XRT: Three doses of 3 Gy. **B.** *In vitro,* the serum stability of L111 in human serum was evaluated by ELISA assay over seven days. The line graph shows the mean±SD of the % of the residual antibody as detected by ELISA assay. **C.** Representative NIR images show L111 uptake in the PDX tumors (white arrows). A PDX from a lung adenocarcinoma patient was established in NSG mice in the right flank. Tumors were either sham-irradiated or irradiated with 3 Gy. IRDye 800 labeled L111 was injected via the tail vein, and whole-body NIR imaging was performed at the indicated time points. **D.** Line graph representing background subtracted NIR signal intensities vs. time post L111 antibody injection. *P<0.05, ***P<0.001, ****P<0.0001

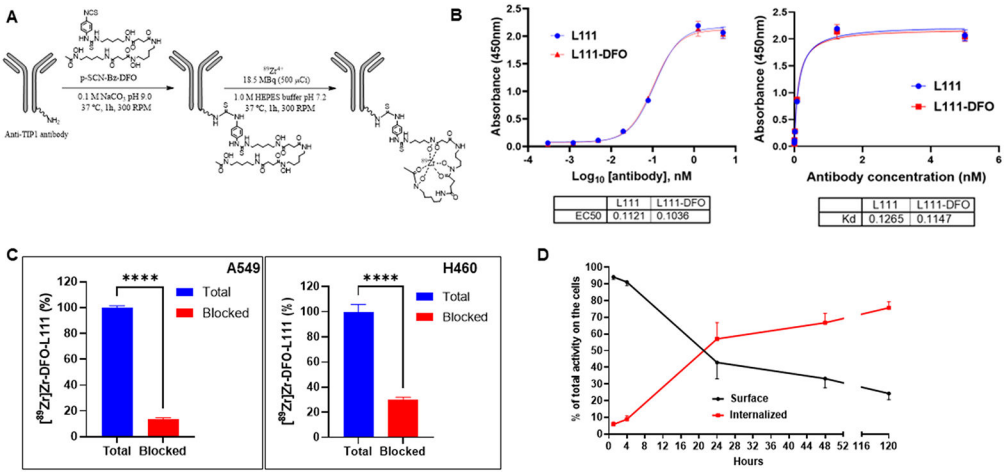

Figure 4. Conjugation of desferoxamine to L111 antibody, radiolabeling, and its characterization.

A. Labeling scheme for the L111 antibody with [^{89}Zr]Zr. The L111 antibody was buffer exchanged (Chelex-treated 0.1 M sodium carbonate/bicarbonate, pH 9.0). DFO was added, and the mixture was allowed to react for 1 h at 37 °C. The reaction mix was buffer exchanged to 1.0 M HEPES buffer. [^{89}Zr]Zr-oxalate was neutralized to ~pH 7.0–7.4 using 1.0 M HEPES pH 7.2 and subsequently mixed with DFO–L111 Ab samples. The reaction mixture was incubated for 60 min at 37 °C at 300 rpm. **B.** ELISA for binding of DFO-L111 to TIP1 protein. Four-fold serial dilutions of the L111 antibodies were incubated with TIP1 protein for indirect ELISA assay. The ELISA data were analyzed using GraphPad Prism software and fitting using log (agonist) vs. response -- Variable slope (four parameters) One Site -- Specific binding. The tables below the graph show the EC50 and K_d values, respectively. **C.** TIP1-specific cell binding of [^{89}Zr]Zr-DFO-L111 was blocked by excess cold L111 (red bars). Bars are mean ± S.**D.** of % bound activity from triplicate samples per group. ****P <0.001. D. Evaluation of cell surface vs. internalized radiolabeled L111 antibody.

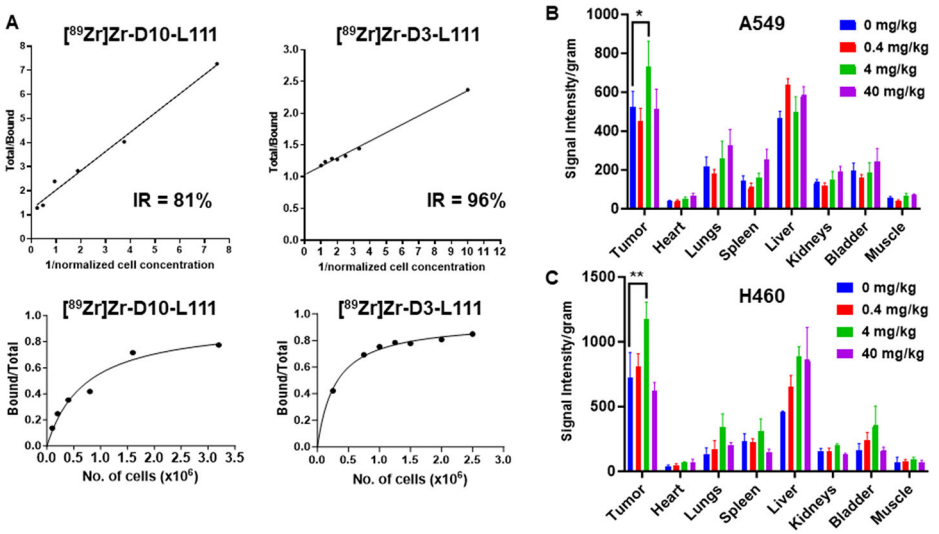

Figure 5. ***In vitro*** **and** ***In vivo*** **evaluation of the L111 antibody.**

A. Immunoreactivity of the [^{89}Zr]Zr-D10-L111 and [^{89}Zr]Zr-D3-L111 on the cancer cell surface. The graphs show the percentage of the immunoreactive fraction. **B and C.** Bar graphs showing Near-infrared signal intensity per gram of the organs harvested from nude mice bearing subcutaneous A549 (B) and H460 (C) tumors (n=3). The mice were injected with 0 to 40 mg/kg unlabeled L111 prior to injecting IRDye800 labeled L111. Organs were harvested after five days of L111 injection. *P<0.05, **P<0.01

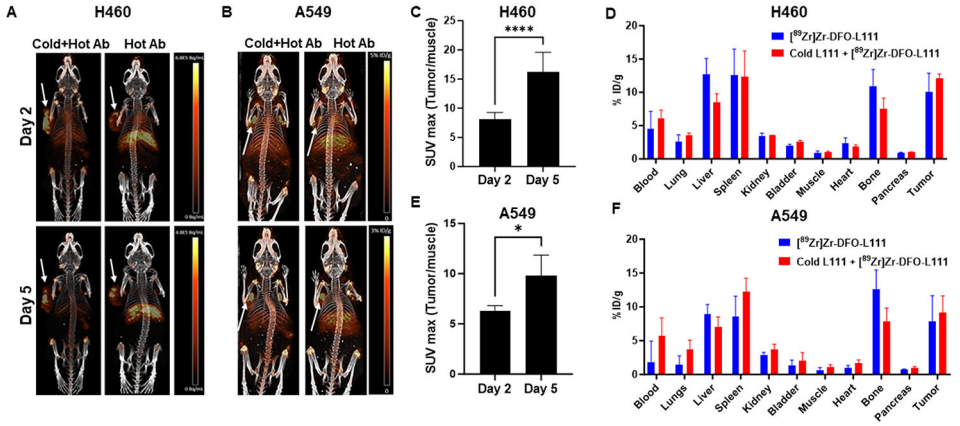

Figure 6. Small animal PET imaging and post-PET biodistribution.

A and B. PET imaging of the mice bearing subcutaneous H460 (A) and A549 (B) tumors (white arrows) injected with either [^{89}Zr]Zr-DFO-L111 antibody or 4 mg/kg cold L111 prior to [^{89}Zr]Zr-DFO-L111 antibody (n=4). Images at days 2 and 5 post-injection are shown. **C.** Bar graph showing the tumor-to-muscle SUVmax values at days 2 and 5 post-injection of the 4 mg/kg cold L111 prior to [^{89}Zr]Zr-DFO-L111 antibody in H460 tumors. **D.** Post-PET biodistribution of the [^{89}Zr]Zr-DFO-L111 antibody and the 4 mg/kg cold L111 injected prior to [^{89}Zr]Zr-DFO-L111 antibody after five days post-injection in H460 tumor-bearing mice. **E.** Bar graph showing the tumor-to-muscle SUVmax values at days 2 and 5 post-injection of the 4 mg/kg cold L111 prior to [^{89}Zr]Zr-DFO-L111 antibody in A549 tumors. **D.** Post-PET biodistribution of the [^{89}Zr]Zr-DFO-L111 antibody and the 4 mg/kg cold L111 injected prior to [^{89}Zr]Zr-DFO-L111 antibody after five days post-injection in A549 tumor-bearing mice.